Hindawi Publishing Corporation
Journal of Nanomaterials
Volume 2013, Article ID 789705, 8 pages
http://dx.doi.org/10.1155/2013/789705

Research Article

Hydrothermal Synthesis and Characterization of Bi_2MoO_6 Nanoplates and Their Photocatalytic Activities

Anukorn Phuruangrat,[1] Pimchanok Jitrou,[1] Phattharanit Dumrongrojthanath,[2] Nuengruethai Ekthammathat,[2] Budsabong Kuntalue,[3] Somchai Thongtem,[4,5] and Titipun Thongtem[2,5]

[1] *Department of Materials Science and Technology, Faculty of Science, Prince of Songkla University, Hat Yai, Songkhla 90112, Thailand*
[2] *Department of Chemistry, Faculty of Science, Chiang Mai University, Chiang Mai 50200, Thailand*
[3] *Electron Microscopy Research and Service Center, Faculty of Science, Chiang Mai University, Chiang Mai 50200, Thailand*
[4] *Department of Physics and Materials Science, Faculty of Science, Chiang Mai University, Chiang Mai 50200, Thailand*
[5] *Materials Science Research Center, Faculty of Science, Chiang Mai University, Chiang Mai 50200, Thailand*

Correspondence should be addressed to Anukorn Phuruangrat; phuruangrat@hotmail.com and Titipun Thongtem; ttpthongtem@yahoo.com

Received 15 June 2013; Revised 17 August 2013; Accepted 26 August 2013

Academic Editor: Jiaguo Yu

The pH effect of the precursor solutions on the phase, morphologies, and photocatalytic activity of Bi_2MoO_6 synthesized by a hydrothermal reaction at 180°C for 20 h was investigated. X-ray powder diffraction (XRD), Raman spectroscopy, Fourier transform infrared (FTIR) spectrometry, scanning electron microscopy (SEM), and transmission electron microscopy (TEM) revealed the presence of pure orthorhombic well-crystallized γ-Bi_2MoO_6 nanoplates, including the symmetric (A_{1g}) and asymmetric (A_{2u}) stretching vibrations of the MoO_6 octahedrons involving the motion of apical oxygen atoms. The photocatalytic activity of Bi_2MoO_6 nanoplates at the pH 6 determined via the decomposition of rhodamine-B (RhB) organic dye was the highest at 98.66% decolorization under Xe light irradiation.

1. Introduction

Photodecomposition of organic compounds and water splitting by semiconducting photocatalysts have attracted the research interest because of the economic situation and environmental ecology for solving energy and pollution problems [1–4]. In the past, the thoroughly conventional studies of TiO_2 displayed its excellent activities and stabilities but the technological application seemed to be limited by some parameters. The most restrictive one is the use of ultraviolet as photonic excitation for the 3.2 eV wide energy gap titania (anatase) [5, 6]. In addition, the solar radiance onto the Earth's surface of less than 5% can be captured by titania, compared to 43% of the visible light [1–3, 7]. Thus the development of a photocatalyst for visible light has become a very interesting topic in the current research on photocatalysis.

Bi-based photocatalysts such as bismuth oxide [8], bismuth vanadate [9, 10], bismuth subcarbonate [11, 12], bismuth tungstate [13], and bismuth molybdate [3, 4] are very important photocatalysts for visible light. Among them, bismuth molybdate as an Aurivillius phase catalyst represented by $(Bi_2O_2)^{2+}(A_{n-1}B_nO_{3n+1})^{2-}$ (A = Ba, Bi, Pb, etc.; B = Ti, Nb, W, Mo, etc.) is composed of unique layered structures with perovskite slabs of $(A_{n-1}B_nO_{3n+1})^{2-}$ sandwiched between $(Bi_2O_2)^{2+}$ layers [3, 14, 15]. Three are three types of pure bismuth molybdates with the phases of α-$Bi_2Mo_3O_{12}$, β-$Bi_2Mo_2O_9$, and γ-Bi_2MoO_6 [16–18], which have been widely studied as potential catalysts to accelerate the decomposition of organic contaminants such as phenol [2], rhodamine B (RhB) [3, 4, 15, 17], n-butene [18], and methylene blue [19, 20] via photogenerated electron-hole pairs [16] by transforming them into CO_2 and H_2O.

In this work, γ-Bi_2MoO_6 nanocrystals were successfully synthesized by a simple hydrothermal method. The as-synthesized γ-Bi_2MoO_6 nanocrystals showed high photocatalytic activity to decompose RhB under visible light radiation.

2. Experimental Procedures

In this research, 0.03 mole of sodium molybdate (Na_2MoO_4) and 0.06 mole of bismuth nitrate ($Bi(NO_3)_3$) were dissolved in 600 mL deionized water. The 600 mL solution was divided into six solutions with 100 mL each. Then HCl (conc.) or 3 M NaOH was added to them until each was achieved at the pH of 2, 4, 6, 8, 10, and 12 with continuous stirring at room temperature. Subsequently, the solutions were hydrothermally processed at 180°C for 20 h to form precipitates. In the end, the as-synthesized precipitates were separated by filtration, rinsed with distilled water and ethanol, and dried at 80°C for 24 h for further characterization.

X-ray powder diffraction (XRD) patterns of the products were recorded on a Japan Rigaku D/MAX-γA X-ray diffractometer with graphite monochromator and Cu K_α radiation (λ = 0.154178 nm) at a scanning rate of 0.02 deg./s ranging from 10 to 60 deg. Raman spectra were recorded on a HORIBA JOBIN YVON T64000 Raman spectrometer at 50 mW and 514.5 nm wavelength Ar green laser and FTIR spectra were recorded on a BRUKER TENSOR 27 Fourier transform infrared (FTIR) spectrometer with KBr as a diluting agent and operated in the range of 400–4,000 cm^{-1}. SEM images were taken on a Hitachi, X650/EDAX, PV9100 scanning electron microscope operating at 35 kV, and TEM images were taken on a JEM 200CX, JEOL transmission electron microscope at an accelerating voltage of 200 kV. UV-visible absorption was carried out on a Lambda 25 PerkinElmer spectrometer, using a quartz cell.

Photocatalytic activities of the as-synthesized samples were tested by measuring the degradation of rhodamine-B (RhB) in an aqueous solution under a visible radiation of Xe lamp. The 150 mg photocatalyst was suspended in a 150 mL of 10^{-5} M RhB aqueous solution, which was magnetically stirred for 30 min in the dark to establish an adsorption-desorption equilibrium of RhB on the surface of the photocatalyst. Then the light was turned on to initiate photocatalysis. The solution was analyzed by a Lambda 25 spectrometer, using 450 W of Xe lamp with wavelength of 553 nm. Decolorization efficiency (%) was calculated using

$$\text{decolorization efficiency } (\%) = \frac{C_o - C}{C_o} \times 100, \quad (1)$$

where C_o is the initial concentration of RhB and C is the concentration of RhB after light irradiation.

3. Results and Discussion

It is well known that the initial pH values of the precursor solutions play an important role in the formation of Aurivillius oxide Bi_2MoO_6 structure. Therefore, solutions with different pH values were used for the present synthesis. The samples synthesized at the pH range from 2 to 12

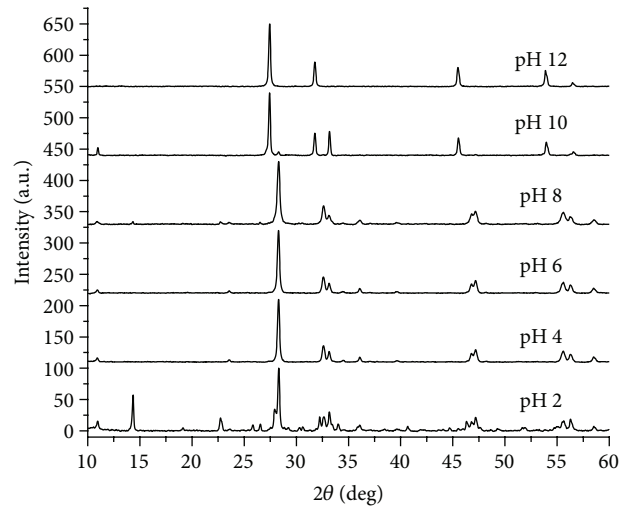

Figure 1: XRD patterns of Bi_2MoO_6 synthesized in the solutions with the pH 2, 4, 6, 8, 10, and 12 by a hydrothermal method.

were classified into three main compositions: Bi_2MoO_6, Bi_2MoO_6/Bi_4MoO_9 composites, and Bi_4MoO_9. The XRD patterns of the as-synthesized products illustrate that low value of pH contributes to the formation of orthorhombic Bi_2MoO_6 structure, medium of pH to mixed phase of orthorhombic Bi_2MoO_6 and cubic Bi_4MoO_9 structures, and high value of pH to the formation of cubic Bi_4MoO_9 structure as shown in Figure 1. XRD pattern of the as-synthesized product at the pH 2 was indexed as mixed phases of Bi_2O_3, MoO_3, Bi_2MoO_6, and so forth. Those at the pH 4 and 6 show an orthorhombic Bi_2MoO_6 with the lattice parameters being determined as a = 5.1896 Å, b = 11.7107 Å, and c = 5.1016 Å corresponding to the database of JCPDS card number 21-0102 [21]. It should be noted that the XRD patterns also indicate the large difference in the relative intensities based on the (020), (131), (200), (002), and (060) peaks for the samples, indicating the possibility of different preferential orientation growth under different pH values. Intensities of the (020) and (060) peaks were much lower than those of the standard, indicating the inhibition of crystalline growth along the [010] direction with the formation of 2D plate-like materials shown by the SEM images. When the pH values were at 8 and 10, the XRD patterns showed mixed phases of Bi_2MoO_6 of the JCPDS number 21-0102 and cubic Bi_4MoO_9 of the JCPDS number 12-0149 [21]. Upon further increase in the pH to 12, the XRD pattern exhibits a pure cubic Bi_4MoO_9 without Bi_2MoO_6 phase detection. On the basis of these results, it can be concluded that the acidic condition favors the formation of Bi_2MoO_6 and that the alkaline medium favors the formation of Bi_4MoO_9.

Bi_2MoO_6 crystal is an orthorhombic structure with $P2_1ab$ space group symmetry at room temperature and ambient pressure and is composed of perovskite-like $(MoO_4)^{2-}$ and fluorite-like $(Bi_2O_2)^{2+}$ layers. For the ideal structure, there are only six Raman active ($2A_{1g} + B_{1g} + 3E_g$) and nine IR active ($4A_{2u} + 5E_u$) modes. These modes are grouped into symmetric and asymmetric stretching vibrations of the MoO_6 octahedrons ($A_{1g} + A_{2u} + E_u$), bending vibrations of the MoO_6

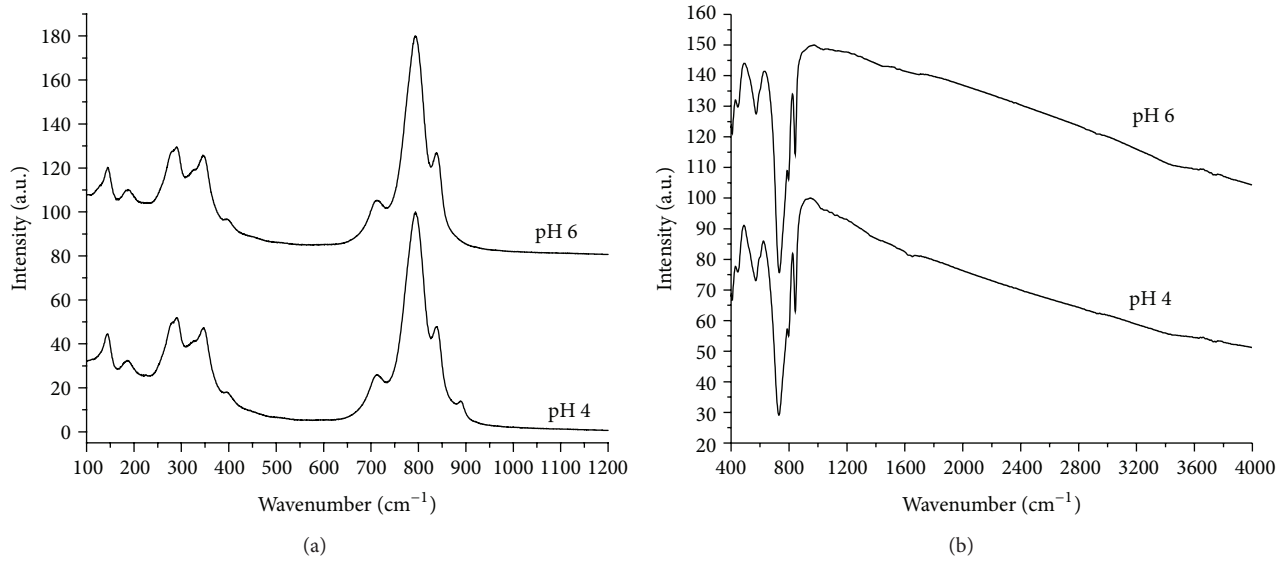

Figure 2: (a) Raman and (b) FTIR spectra of Bi_2MoO_6 synthesized in the solutions with the pH 4 and 6 by a hydrothermal method.

octahedrons ($E_g + 2E_u + A_{2u} + B_{2u}$), stretching and bending vibrations of the $(Bi_2O_2)^{2+}$ layers ($B_{1g} + E_g + A_{2u} + E_u$), translation motions of Bi atoms ($A_{1g} + E_g$), and vibrations involving translation motions of Bi and Mo atoms ($A_{2u} + E_u$). Due to orthorhombic distortion, all of the nondegenerate and degenerate modes are split, including the generation of new modes at lower wavenumber. Thus overall modes become $26A_1 + 27A_2 + 26B_1 + 26B_2$. Selection rules state that the A_1, B_1, and B_2 modes are both Raman and IR active, but the A_2 modes are only Raman active [22, 23]. Raman spectra of Bi_2MoO_6 samples synthesized at the pH 4 and 6 by the hydrothermal method are shown in Figure 2(a). They were classified into three regions: <180 cm^{-1}, 180–500 cm^{-1}, and 700–850 cm^{-1}. The modes below 180 cm^{-1} could be the translation of molybdenum and bismuth atoms. Vibration peak at 144 cm^{-1}, specified as the lattice mode of Bi^{3+} atoms, was mainly in the direction normal to the layers. It is well known that the peaks in the 180–500 cm^{-1} range originated from bending modes of the MoO_6 octahedrons coupled with stretching and bending modes of the bismuth-oxygen polyhedrons. The intense Raman modes near 290 and 280 cm^{-1} seemed to be from the E_g bending vibrations. Those at 323, 345, and 398 cm^{-1} corresponded to the E_u symmetric bending. The mode at 712 cm^{-1}, exhibiting no evident shift or broadness, was specified as the asymmetric stretching vibration (E_u mode) of the MoO_6 octahedrons involving the motion of equatorial oxygen atoms joining the MoO_6 octahedrons within the layers. The Raman vibrations at 793 cm^{-1} (A_{1g} mode) and 840 cm^{-1} (A_{2u} mode) were, respectively, assigned to the symmetric and asymmetric stretching vibrations of the MoO_6 octahedrons involving the motion of apical oxygen atoms, normally directed to the $(Bi_2O_2)^{2+}$ layers [3, 15, 22, 24].

Figure 2(b) shows the FTIR spectra of Bi_2MoO_6 samples obtained by hydrothermal reactions at the pH 4 and 6. The main absorption bands at 400–950 cm^{-1} are mainly related to Bi–O and Mo–O stretching and Mo–O–Mo bridging stretching modes. The bands at 843 and 797 cm^{-1} were, respectively, assigned as the asymmetric and symmetric stretching modes of MoO_6 involving vibrations of apical oxygen atoms. The 734 cm^{-1} mode was attributed to the asymmetric stretching mode of MoO_6 involving vibrations of the equatorial oxygen atoms. Those at 603 and 570 cm^{-1} corresponded to the bending vibrations of MoO_6. Furthermore, a small band at 454 cm^{-1} was attributed to the stretching and bending vibrations of BiO_6 octahedrons [3, 24].

Figure 3 shows SEM images of the Bi_2MoO_6 samples synthesized in the solutions with the pH of 4 and 6 by the hydrothermal method at 180°C for 24 h. The low-magnification SEM images of both samples showed that the as-synthesized Bi_2MoO_6 samples were composed of uniform plate-like structures ranging from 100 nm to 200 nm. The corresponding high-magnification SEM images demonstrated close-up views of the individual disks which clearly revealed the presence of orderly packed square nanoplates with their thickness of about several nanometers and the average length of 200–400 nm. The higher pH value seemed to produce smaller crystallites, which led to higher surface areas.

To reveal morphology of the as-synthesized Bi_2MoO_6, the samples were characterized by TEM as shown in Figure 4. The γ-Bi_2MoO_6 sample at the pH 4 was composed of square nanoplates with thin edge. But for the pH of 6, they exhibited an explicit one. The selected area electron diffraction (SAED) patterns of individual Bi_2MoO_6 nanoplates present regular square diffraction spot array, revealing the single-crystalline nanoplates. In the present analysis, both SAED patterns can be indexed as (060), (062), and (002) planes with the [100] direction as zone axis of orthorhombic Bi_2MoO_6 structure. It should be noted that both diffraction patterns were composed of a number of diffraction spots arranged in systematic arrays. Weak diffraction spots, due to the high-order Laue

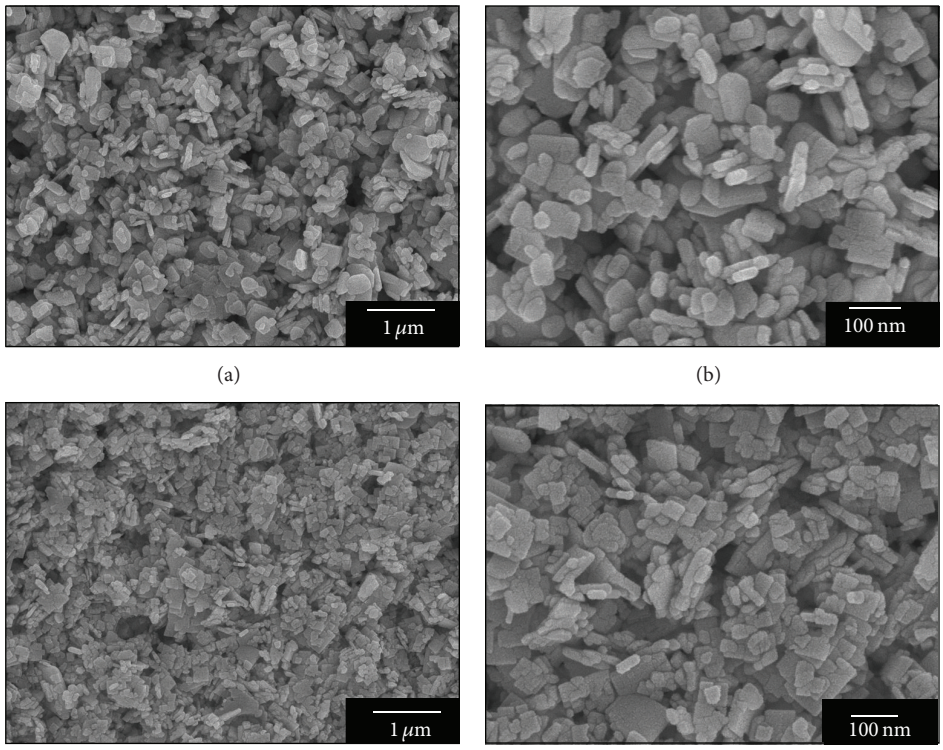

Figure 3: SEM images at low and high magnifications of Bi_2MoO_6 synthesized in the solutions with the pH ((a), (b)) 4 and ((c), (d)) 6 by a hydrothermal method.

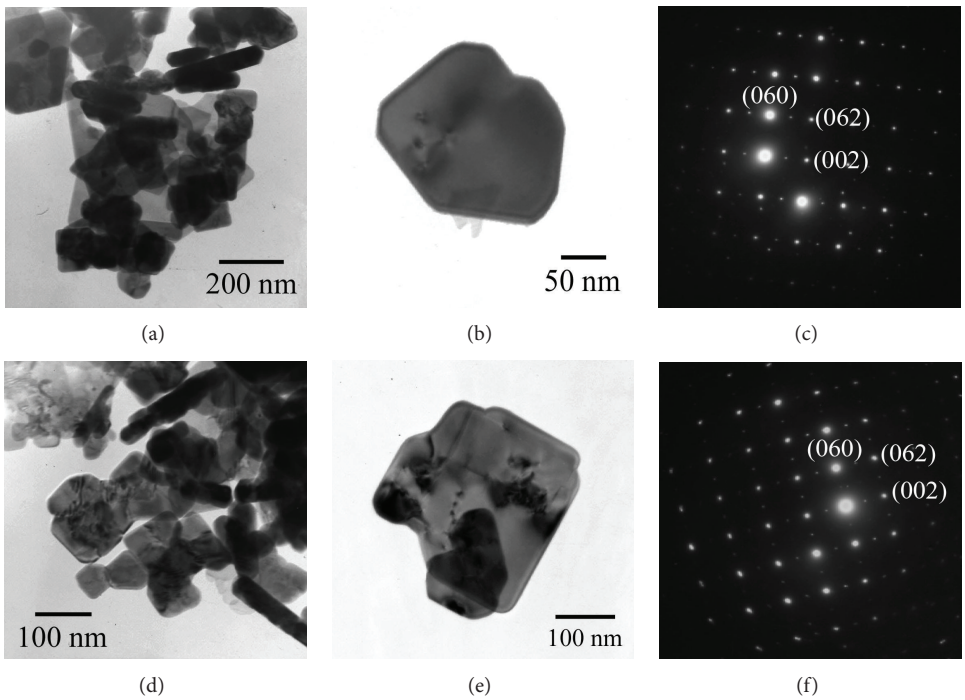

Figure 4: TEM images and SAED patterns of Bi_2MoO_6 synthesized in the solutions with the pH ((a)–(c)) 4 and ((d)–(f)) 6 by a hydrothermal method.

zone caused by the combined effects of the lengthened diffraction spots in the direction normal to the nanolayers and the narrow Laue zone along the [002] direction, were also detected in the forbidden sites [4]. When the center of the circular arc of Ewald sphere does not coincide with bright spots of the transmitted beam, asymmetrical patterns will be detected. A symmetrical pattern is obtainable for a precise zone axis orientation, at which the center of the arc coincides with the spots of the transmitted beam [25].

It has been reported that orthorhombic Bi_2MoO_6 is constructed by corner-shared MoO_6 octahedral layers with their edges directing along the [100] and [001] directions and $(Bi_2O_2)^{2+}$ layers sandwiched between MoO_6 octahedral layers. Therefore, the direction of the nanolayers stacking is along the [010] direction normal to the [100] and [001] directions of the planes. Based on the experimental results, it can be concluded that under low pH value, there existed higher surface energy on the (100) and (001) planes compared with others. The growth of nanocrystals along the [010] direction was inhibited. The cleavages on surfaces of Bi_2MoO_6 crystal also provide information for explaining the adsorption of H^+ cations. The (100), (010), and (001) crystal planes are terminated by the Mo, O, and Bi atoms, respectively. The zigzag orientations of Mo octahedral anions on the (100) faces induce these faces to become unfavorable for the adsorption of H^+ cations. The amount of O atoms on the (010) planes was much higher than others. H^+ cations preferred to adsorb on the (010) planes due to the high density of oxygen atoms on these faces. Thus the crystal growth along the [010] direction slowed down, including nanoplates formed [24, 26].

Figure 5 displays UV-visible absorption spectra of Bi_2MoO_6 nanoplates, which have strong photoabsorption properties ranging from ultraviolet to visible light with the wavelength being shorter than 500 nm. The steep shape of the absorption edge corresponded to the intrinsic energy gap transition of Bi_2MoO_6 ranging from the valence band of the O 2p orbitals to the conduction band derived from the primary Mo 4d orbitals in MoO_6 octahedrons and the secondary Bi 6p orbitals [27, 28]. Their absorption edge wavelengths were determined to be 435–445 nm which were appropriate for the photocatalysis to accelerate the degradation of organic contaminants under UV-visible range.

To study the photocatalytic activities of the hydrothermally synthesized samples, tetraethylated rhodamine (RhB) with a major absorption band at 553 nm was chosen as a model organic contaminant. A change in the UV-visible spectra of the aqueous RhB solutions during photocatalytic decolorization using the Bi_2MoO_6 nanoplates at the pH 4 and pH 6 is presented in Figure 6. During 180 min testing, the absorption intensity of RhB at 553 nm was gradually decreased and shifted towards the blue region from 553 nm to 498 nm with the formation of deethylated RhB molecules [15, 29, 30]. The fully N,N,N′,N′-tetraethylated rhodamine molecules (553 nm) show deethylation step by step to N,N,N′-triethylated rhodamine (539 nm), N,N′-diethylated rhodamine (522 nm), N-ethylated rhodamine (510 nm), and rhodamine (498 nm) [3, 13, 15]; the remains were degraded through the decomposition of conjugated structure. At the completion of visible irradiation for 180 min, the absorption

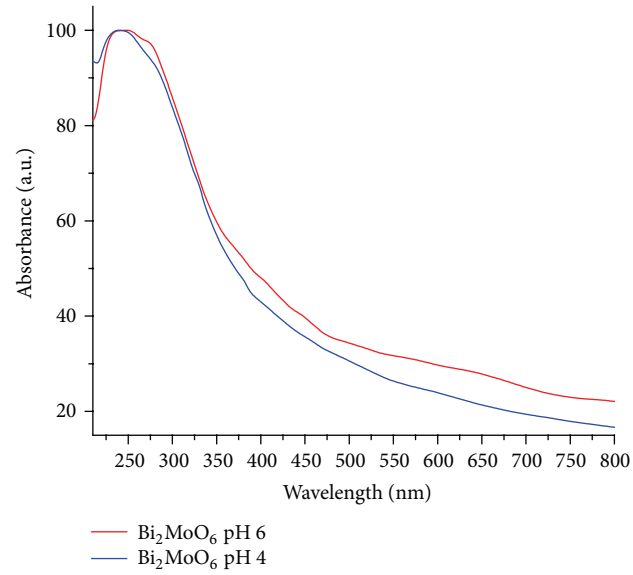

FIGURE 5: UV-visible absorption of Bi_2MoO_6 nanoplates synthesized in the solutions with the pH 4 and 6 by a hydrothermal method.

intensity of RhB aqueous solution became very weak. The RhB solution could turn into a colorless one by further increase in the length of time to longer than 180 min. It should be noted that the content of RhB was exponentially reduced with the increase in the length of irradiation time [2]. Thus the RhB content will reach zero concentration at the irradiation time of infinity, and the decolorization of RhB was complete.

Figure 7 displays the degradation process of RhB in the solutions containing Bi_2MoO_6 synthesized at the pH of 4 and 6 as a photocatalyst, compared to that without Bi_2MoO_6. For the controlled solution, RhB did not degrade both in the dark and in the illuminated condition. In the present research, visible light was essential to the RhB photodegradation. Bi_2MoO_6 at the pH 6 showed significantly better photocatalytic degradation properties than Bi_2MoO_6 at the pH 4. The pH of the precursors for the formation of Bi_2MoO_6 nanoplates was found to strongly affect the photocatalytic efficiency. The photodegradation using Bi_2MoO_6 at the pH 6 reached 98.66% within 180 min under visible-light irradiation, resulting from the smaller crystallites and larger specific surface areas [31]. Compared with P25 TiO_2, the degradation of RhB under the visible light irradiation was 18% within 120 min [32]. Thus Bi_2MoO_6 was claimed to be a potential photocatalyst under visible light.

Based on the photocatalytic degradation of organic compounds in the solutions containing Bi_2MoO_6, a possible mechanism was proposed [9, 33–35]. At the beginning, the γ-Bi_2MoO_6 photocatalyst absorbed visible light to generate electron-hole pairs. The electrons ($BMO(e_{cb}^-)$) at the Bi_2MoO_6 surfaces were scavenged by the adsorbed molecular oxygen and the $O_2\bullet^-$ superoxide radical anions formed. RhB molecules could also absorb visible light in the 460–600 nm range. Thus RhB molecules were excited by being transformed into activated molecules (RhB^*). The electrons diffused from the activated chemisorbed RhB_{ad}^* molecules

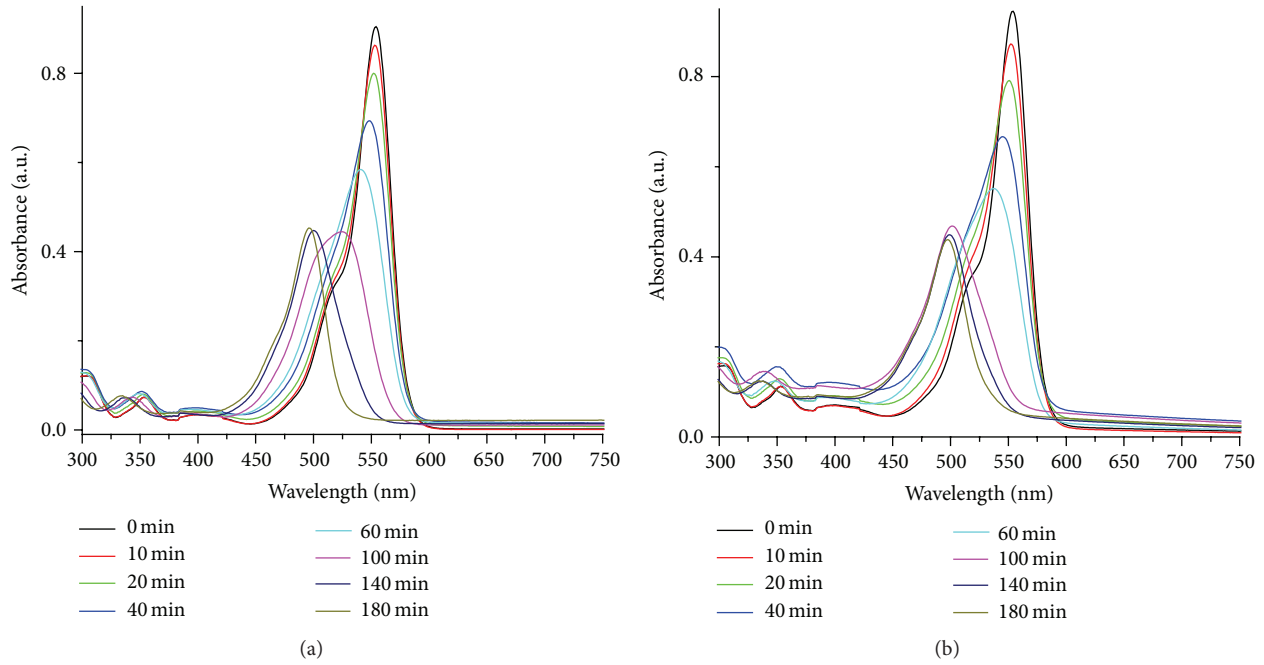

Figure 6: UV-visible absorption of RhB in the solutions containing Bi_2MoO_6 nanoplates synthesized at the pH (a) 4 and (b) 6.

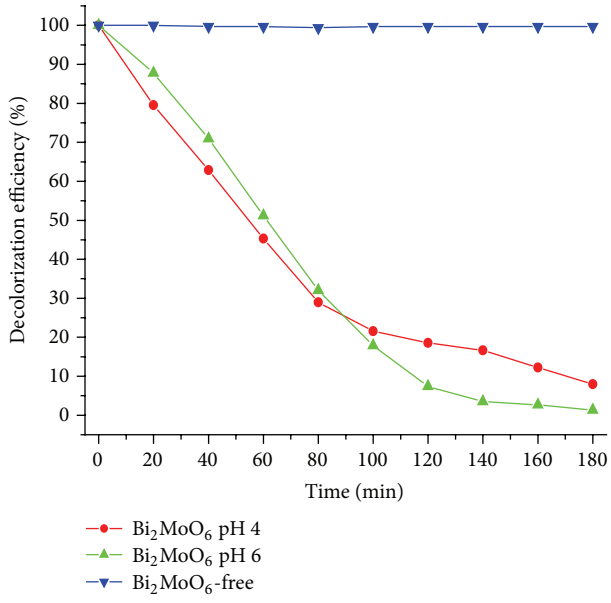

Figure 7: Decolorization efficiencies of RhB in the solutions containing Bi_2MoO_6 nanoplates synthesized at the pH 4 and 6 compared to the catalyst-free solution under Xe light.

to the Bi_2MoO_6 surfaces, which were immediately released into the conduction band of Bi_2MoO_6 to generate BMO(e_{cb}^-) and further reacted with the surface adsorbed oxygen to generate $O_2\bullet^-$ superoxide radicals. Concurrently, BMO(h_{vb}^+) combined with water molecules and/or hydroxyl ions to form OH• radicals. Then all deethylated intermediates were further degraded by both of the radicals. It should be noted that there was a competition between the deethylation and the decomposition of conjugated structure proceeding on the surfaces of the Bi_2MoO_6 samples:

$$Bi_2MoO_6 + hv \longrightarrow BMO\left(e_{cb}^-\right) + BMO\left(h_{vb}^+\right) \quad (2)$$

$$BMO\left(e_{cb}^-\right) + O_2 \longrightarrow O_2\bullet^- + Bi_2MoO_6 \quad (3)$$

$$RhB + hv \longrightarrow RhB^* \quad (4)$$

$$RhB_{ad}^* + BMO \longrightarrow RhB\bullet^+ + BMO\left(e_{cb}^-\right) \quad (5)$$

$$H_2O \text{ or } OH + BMO\left(h_{vb}^+\right) \longrightarrow OH\bullet \quad (6)$$

$$RhB\bullet^+ + O_2\bullet^- \longrightarrow \text{subproducts} \quad (7)$$

4. Conclusions

The present research was to study the effect of pH on phase, morphologies, and photocatalytic properties of orthorhombic Bi_2MoO_6 nanoplates synthesized by the hydrothermal method at 180°C for 20 h. Based on the various characterization techniques, the appropriate condition for the synthesis of orthorhombic Bi_2MoO_6 nanoplates was at the pH 4 and 6. The photocatalytic activity of Bi_2MoO_6 nanoplates at the pH 6 was determined to be the highest at 98.66% degradation of RhB under Xe radiation for 180 min.

Acknowledgment

The authors are extremely grateful to the Prince of Songkla University, Hat Yai, Songkhla, Thailand, for providing financial support through the Contact no. SCI560002S.

References

[1] P. Wang, Y. Ao, C. Wang, J. Hou, and J. Qian, "A one-pot method for the preparation of graphene-Bi_2MoO_6 hybrid photocatalysts that are responsive to visible-light and have excellent photocatalytic activity in the degradation of organic pollutants," *Carbon*, vol. 50, pp. 5256–5264, 2012.

[2] W. Yin, W. Wang, and S. Sun, "Photocatalytic degradation of phenol over cage-like Bi_2MoO_6 hollow spheres under visible-light irradiation," *Catalysis Communications*, vol. 11, no. 7, pp. 647–650, 2010.

[3] H. Li, C. Liu, K. Li, and H. Wang, "Preparation, characterization and photocatalytic properties of nanoplate Bi_2MoO_6 catalysts," *Journal of Materials Science*, vol. 43, no. 22, pp. 7026–7034, 2008.

[4] H. Yu, Z. Zhu, J. Zhou, J. Wang, J. Li, and Y. Zhang, "Self-assembly and enhanced visible-light-driven photocatalytic activities of Bi_2MoO_6 by tungsten substitution," *Applied Surface Science*, vol. 265, pp. 424–430, 2013.

[5] R. Asahi, T. Morikawa, T. Ohwaki, K. Aoki, and Y. Taga, "Visible-light photocatalysis in nitrogen-doped titanium oxides," *Science*, vol. 293, no. 5528, pp. 269–271, 2001.

[6] J. Yu, G. Dai, Q. Xiang, and M. Jaroniec, "Fabrication and enhanced visible-light photocatalytic activity of carbon self-doped TiO_2 sheets with exposed 001 facets," *Journal of Materials Chemistry*, vol. 21, no. 4, pp. 1049–1057, 2011.

[7] T. Zhou, J. Hu, and J. Li, "Er^{3+} doped bismuth molybdate nanosheets with exposed 010 facets and enhanced photocatalytic performance," *Applied Catalysis B*, vol. 110, pp. 221–230, 2011.

[8] X. Xiao, R. Hu, C. Liu et al., "Facile large-scale synthesis of β-Bi_2O_3 nanospheres as a highly efficient photocatalyst for the degradation of acetaminophen under visible light irradiation," *Applied Catalysis B*, vol. 140-141, pp. 433–443, 2013.

[9] B. Cheng, W. Wang, L. Shi, J. Zhang, J. Ran, and H. Yu, "One-pot template-free hydrothermal synthesis of monoclinic $BiVO_4$ hollow microspheres and their enhanced visible-light photocatalytic activity," *International Journal of Photoenergy*, vol. 2012, Article ID 797968, 10 pages, 2012.

[10] P. Madhusudan, J. Ran, J. Zhang, J. Yu, and G. Liu, "Novel urea assisted hydrothermal synthesis of hierarchical $BiVO_4/Bi_2O_2CO_3$ nanocomposites with enhanced visible-light photocatalytic activity," *Applied Catalysis B*, vol. 110, pp. 286–295, 2011.

[11] H. Y. Liang, Y. X. Yang, J. C. Tang, and M. Ge, "Photocatalytic properties of $Bi_2O_2CO_3$ nanosheets synthesized via a surfactant-assisted hydrothermal method," *Materials Science in Semiconductor Processing*, vol. 16, pp. 1650–1654, 2013.

[12] P. Madhusudan, J. Yu, W. Wang, B. Cheng, and G. Liu, "Facile synthesis of novel hierarchical graphene-$Bi_2O_2CO_3$ composites with enhanced photocatalytic performance under visible light," *Dalton Transactions*, vol. 41, pp. 14345–14353, 2012.

[13] P. Dumrongrojthanath, T. Thongtem, A. Phuruangrat, and S. Thongtem, "Hydrothermal synthesis of Bi_2WO_6 hierarchical flowers with their photonic and photocatalytic properties," *Superlattices and Microstructures*, vol. 54, pp. 71–77, 2013.

[14] J. Ren, W. Wang, M. Shang, S. Sun, and E. Gao, "Heterostructured bismuth molybdate composite: preparation and improved photocatalytic activity under visible-light irradiation," *ACS Applied Materials and Interfaces*, vol. 3, no. 7, pp. 2529–2533, 2011.

[15] H. Li, K. Li, and H. Wang, "Hydrothermal synthesis and photocatalytic properties of bismuth molybdate materials," *Materials Chemistry and Physics*, vol. 116, no. 1, pp. 134–142, 2009.

[16] X. Zhao, H. Liu, Y. Shen, and J. Qu, "Photocatalytic reduction of bromate at C_{60} modified Bi_2MoO_6 under visible light irradiation," *Applied Catalysis B*, vol. 106, no. 1-2, pp. 63–68, 2011.

[17] E. L. Cuéllar, A. Martínez-De La Cruz, K. H. L. Rodríguez, and U. O. Méndez, "Preparation of γ-Bi_2MoO_6 thin films by thermal evaporation deposition and characterization for photocatalytic applications," *Catalysis Today*, vol. 166, no. 1, pp. 140–145, 2011.

[18] J. C. Jung, H. Lee, D. R. Park, J. G. Seo, and I. K. Song, "Effect of calcination temperature on the catalytic performance of γ-Bi_2MoO_6 in the oxidative dehydrogenation of n-butene to 1,3-butadiene," *Catalysis Letters*, vol. 131, no. 3-4, pp. 401–405, 2009.

[19] R. Gruar, C. J. Tighe, L. M. Reilly, G. Sankar, and J. A. Darr, "Tunable and rapid crystallisation of phase pure Bi_2MoO_6 (koechlinite) and $Bi_2Mo_3O_{12}$ via continuous hydrothermal synthesis," *Solid State Sciences*, vol. 12, no. 9, pp. 1683–1686, 2010.

[20] H. Xie, D. Shen, X. Wang, and G. Shen, "Microwave hydrothermal synthesis and visible-light photocatalytic activity of γ-Bi_2MoO_6 nanoplates," *Materials Chemistry and Physics*, vol. 110, no. 2-3, pp. 332–336, 2008.

[21] Powder Diffraction File, JCPDS-ICDD, 12 Campus Boulevard, Newtown Square, Pa, USA, 19073-3273, 2001.

[22] M. MacZka, P. T. C. Freire, C. Luz-Lima, W. Paraguassu, J. Hanuza, and J. Mendes Filho, "Pressure-induced phase transitions in ferroelectric Bi_2MoO_6—a Raman scattering study," *Journal of Physics Condensed Matter*, vol. 22, no. 1, Article ID 015901, 2010.

[23] M. Mączka, L. Macalik, K. Hermanowicz, L. Kępiński, and J. Hanuza, "Synthesis and phonon properties of nanosized aurivillius phase of Bi_2MoO_6," *Journal of Raman Spectroscopy*, vol. 41, no. 10, pp. 1289–1296, 2010.

[24] L. Zhang, T. Xu, X. Zhao, and Y. Zhu, "Controllable synthesis of Bi_2MoO_6 and effect of morphology and variation in local structure on photocatalytic activities," *Applied Catalysis B*, vol. 98, no. 3-4, pp. 138–146, 2010.

[25] B. Fultz and J. M. Howe, *Transmission Electron Microscopy and Diffractometry of Materials*, Springer, Heidelberg, Germany, 3rd edition, 2007.

[26] L. Zhang and Y. Zhu, "A review of controllable synthesis and enhancement of performances of bismuth tungstate visible-light-driven photocatalysts," *Catalysis Science and Technology*, vol. 2, no. 4, pp. 694–706, 2012.

[27] T. Zhang, J. Huang, S. Zhou, H. Ouyang, L. Cao, and A. Li, "Microwave hydrothermal synthesis and optical properties of flower-like Bi_2MoO_6 crystallites," *Ceramics International*, vol. 39, pp. 7391–7394, 2013.

[28] J. Bi, J. Che, L. Wu, and M. Liu, "Effects of the solvent on the structure, morphology and photocatalytic properties of Bi_2MoO_6 in the solvothermal process," *Materials Research Bulletin*, vol. 48, pp. 2071–2075, 2013.

[29] J. Bi, L. Wu, J. Li, Z. Li, X. Wang, and X. Fu, "Simple solvothermal routes to synthesize nanocrystalline Bi_2MoO_6 photocatalysts with different morphologies," *Acta Materialia*, vol. 55, no. 14, pp. 4699–4705, 2007.

[30] L. Xie, J. Ma, and G. Xu, "Preparation of a novel Bi_2MoO_6 flake-like nanophotocatalyst by molten salt method and evaluation for photocatalytic decomposition of rhodamine B," *Materials Chemistry and Physics*, vol. 110, no. 2-3, pp. 197–200, 2008.

[31] J. Yu, Y. Su, B. Cheng, and M. Zhou, "Effects of pH on the microstructures and photocatalytic activity of mesoporous nanocrystalline titania powders prepared via hydrothermal method," *Journal of Molecular Catalysis A*, vol. 258, no. 1-2, pp. 104–112, 2006.

[32] X. Cheng, X. Yu, Z. Xing, and L. Yang, "Enhanced visible light photocatalytic activity of mesoporous anatase TiO_2 codoped with nitrogen and chlorine," *International Journal of Photoenergy*, vol. 2012, Article ID 593245, 6 pages, 2012.

[33] Y. Zheng, F. Duan, J. Wu, L. Liu, M. Chen, and Y. Xie, "Enhanced photocatalytic activity of bismuth molybdates with the preferentially exposed 010 surface under visible light irradiation," *Journal of Molecular Catalysis A*, vol. 303, no. 1-2, pp. 9–14, 2009.

[34] Q. Xiang, J. Yu, and P. K. Wong, "Quantitative characterization of hydroxyl radicals produced by various photocatalysts," *Journal of Colloid and Interface Science*, vol. 357, no. 1, pp. 163–167, 2011.

[35] K.-I. Ishibashi, A. Fujishima, T. Watanabe, and K. Hashimoto, "Detection of active oxidative species in TiO_2 photocatalysis using the fluorescence technique," *Electrochemistry Communications*, vol. 2, no. 3, pp. 207–210, 2000.